Coupled-state calculations of proton–hydrogen-atom scattering using a scaled hydrogenic basis set

Robin Shakeshaft
Physics Department, Texas A&M University, College Station, Texas 77843
(Received 1 June 1978)

Coupled-state calculations of proton–hydrogen-atom scattering using a scaled hydrogenic basis set have been performed, and the results are reported on in this paper. Thirty-five basis functions, centered about each proton, were included in the expansion of the electron wave function. Cross sections for direct excitation and charge transfer to the $n = 1$, 2, and 3 levels, and for ionization, have been calculated. The results for ionization indicate that charge transfer to the continuum dominates over direct ionization at proton energies below about 60 keV. The charge distribution has been plotted as a function of time at an energy of 40 keV and impact parameter of 1.5 a.u.; the plot illustrates the considerable distortion of the electron cloud caused by the passing proton.

I. INTRODUCTION

It is the purpose of this paper to report new results of calculations of cross sections for proton–hydrogen-atom scattering. These results were obtained by solving the standard time-dependent impact-parameter coupled-state equations for the electron wavefunction using an expansion in scaled hydrogenic functions,

$$\phi_{nlm}(\vec{r}) = R_{nl}(\lambda_{nl} r)[Y_{lm}(\hat{r}) + Y^*_{lm}(\hat{r})] ,$$

which satisfy the equation (adopting atomic units)

$$(-\tfrac{1}{2}\nabla^2_{\vec{r}} - \lambda_{nl}/r + \tfrac{1}{2}\lambda^2_{nl}/n^2)\phi_{nlm}(\vec{r}) = 0 .$$

The expansion included 35 such functions centered about each proton, with $0 \leq l \leq 2$, $0 \leq m \leq l$, and $l \leq n \leq N_l$ where $N_0 = 9$, $N_1 = 8$, $N_2 = 6$. The scale factors λ_{nl} were chosen as follows: $\lambda_{n0} = 0.75n$, $\lambda_{n1} = 0.7n$, $\lambda_{n2} = 0.6n$. Note that the Sturmian functions, which have been used in previous coupled-state calculations,[1,2] are obtained by setting $\lambda_{nl} = n/(l+1)$, and the hydrogen-atom wave functions, which have also been used in previous calculations,[3–6] are obtained by setting $\lambda_{nl} = 1$. The present choice of scale factors was determined by the requirement that when the hydrogen-atom Hamiltonian, $-\frac{1}{2}\nabla^2_{\vec{r}} - 1/r$, is diagonalized in the space spanned by the $\phi_{nlm}(\vec{r})$, the resulting energy eigenvalues almost coincide with the energies of the $1s$, $2s$, $2p$, $3s$, $3p$, and $3d$ states *and* overlap the low-energy part of the continuous spectrum of the hydrogen atom. The eigenvalues of the diagonalized Hamiltonian are shown in Table I. The electron wave function was, in fact, expanded in the eigenvectors that diagonalize the hydrogen-atom Hamiltonian, rather than in the basis functions ϕ_{nlm}; if the number of eigenvectors were equal to the number of basis functions there would be no difference between the two expansions, but in the present calculations the eigenvector corresponding to the large $9s$ eigenvalue shown in Table I was omitted from the expansion since it does not play a very significant role. Thus 34 eigenvectors, centered about each proton, were included in the expansion of the electron wave function.

The numerical methods which made it possible to perform the present rather elaborate calculations have been described elsewhere,[2,7] and will not be discussed here. However, one new feature not discussed in Refs. 2 and 7 is the use of an assembly language routine to perform matrix multiplications. This routine was written by Stephen P. Rountree. Note that the method described in Ref. 7 for evaluating matrix elements in the Sturmian representation may be readily generalized to the evaluation of matrix elements in the

TABLE I. The eigenvalues of the hydrogen-atom Hamiltonian when diagonalized in the space of scaled hydrogenic functions $\phi_{nlm}(r)$. The principal quantum number n in this table serves to order the eigenvalues, with $n-l-1$ being equal to the number of nodes in the corresponding eigenvectors. The eigenvalues are in atomic units.

n \ l	0	1	2
1	−0.500		
2	−0.125	−0.125	
3	−0.0552	−0.0552	−0.0551
4	−0.0163	−0.0158	−0.0119
5	0.0541	0.0595	0.0967
6	0.199	0.227	0.507
7	0.532	0.678	
8	1.552	2.612	
9	7.640		

present representation since the present scale factors λ_{nl} are, for a fixed l, proportional to n. Furthermore, since the λ_{nl} are proportional to n the entire discrete set of the present scaled hydrogenic functions is complete. Thus the present basis functions share the merits of the Sturmian functions. The advantage of the present basis functions over the Sturmian functions is that they provide a better representation of the first few excited states and the low-energy part of the continuum of the hydrogen atom.

II. RESULTS AND DISCUSSION

In Table II are presented the total cross sections for direct excitation and charge transfer to the lowest three levels and for ionization. I first discuss direct excitation to the $n=2$ level. In Fig. 1 are plotted the present results for the total cross section for direct excitation to the $n=2$ level, along with the experimental results of Park *et al.*,[8] as well as the theoretical estimates I obtained previously[2] from coupled-state calculations based on an expansion in 12 Sturmian functions centered about each proton. I have normalized the experimental results to the present theoretical results at 200 keV. In the earlier Sturmian calculation d states were not included and this accounts for the discrepancy between the Sturmian results and the present results at energies above 70 keV. The dip in the present results at about 55 keV is almost certainly artificial, and may be due to the inability of the scaled hydrogenic functions to account for ionization sufficiently well.[2] The ioni-

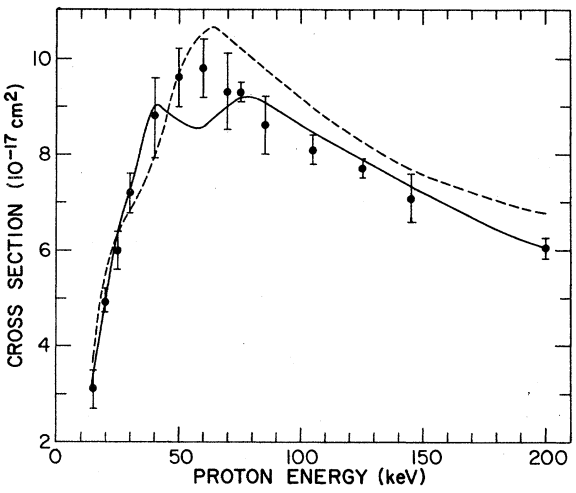

FIG. 1. Total cross sections for direct excitation to the $n=2$ level. ——, present 34-state results; — — —, earlier 12-state Sturmian results (Ref. 2); ●, experimental results of Park *et al.* (Ref. 8). The experimental results have been normalized to the present results at 200 keV; thus the experimental data of Ref. 8 should be multiplied by a factor of 0.91.

TABLE II. Estimates of the total cross sections for direct excitation and charge transfer in units of 10^{-17} cm^2. Rows *a* refer to excitation and rows *b* to charge transfer. The last column includes the contribution to the ionization cross section from both direct ionization and charge transfer to the continuum. The quantization axis is the beam axis.

Energy (keV)		Final state: $1s$	$2s$	$2p_0$	$2p_1$	$3s$	$3p_0$	$3p_1$	$3d_0$	$3d_1$	$3d_2$	Continuum
15	*a*		0.88	1.00	1.46	0.18	0.18	0.29	0.082	0.12	0.011	3.1
	b	58.35	3.41	0.94	2.16	0.53	0.33	0.41	0.050	0.14	0.008 9	
25	*a*		1.56	1.96	2.89	0.44	0.40	0.46	0.17	0.13	0.036	8.5
	b	30.35	3.98	0.76	0.98	0.93	0.28	0.24	0.031	0.025	0.004 5	
40	*a*		2.10	3.12	3.77	0.37	0.42	0.75	0.13	0.27	0.043	14.6
	b	11.89	2.33	0.38	0.34	0.67	0.13	0.11	0.015	0.009 1	0.001 5	
50	*a*		1.79	2.69	4.19	0.44	0.63	0.77	0.26	0.19	0.038	15.9
	b	6.78	1.39	0.23	0.17	0.45	0.077	0.058	0.017	0.005 7	0.000 8	
60	*a*		1.32	2.60	4.69	0.38	0.55	0.77	0.25	0.087	0.049	16.0
	b	4.10	0.82	0.12	0.089	0.29	0.058	0.030	0.017	0.003 0	0.000 4	
75	*a*		1.19	3.07	4.90	0.28	0.33	0.88	0.065	0.11	0.057	15.0
	b	2.10	0.42	0.049	0.037	0.14	0.018	0.012	0.002 6	0.001 0	0.000 2	
145	*a*		0.80	2.37	4.16	0.13	0.40	0.80	0.031	0.082	0.039	9.4
	b	0.19	0.040	0.0054	0.0023	0.012	0.0017	0.0008	0.001 0	0.000 1	0.000 02	
200	*a*		0.49	1.71	3.84	0.11	0.30	0.69	0.029	0.031	0.034	6.5
	b	0.047	0.0087	0.0010	0.0004	0.0030	0.0004	0.0001	0.000 04	0.000 02	0.000 002	

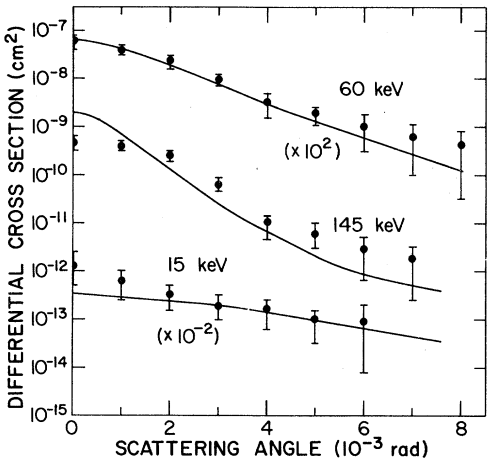

FIG. 2. Differential cross sections, in the center of mass frame, for direct excitation to the $n=2$ level at selected lab energies. ——, present theoretical results; ●, experimental results of Park *et al.* (Ref. 10, renormalized as in Fig. 1).

zation cross section peaks at about 55 keV, and is very large there. Consequently the flux into those eigenvectors overlapping the continuum is large. However, this flux cannot escape to infinity since the electron, in attempting to escape, encounters artificial barriers erected because the eigenvectors, being square integrable, extend over only finite distances. Thus some electron flux that should escape to infinity may be induced back into the bound-state channels as the collision progresses. (Of course, transitions between the ionization and bound-state channels eventually cease since the perturbation vanishes.) Aside from the region 40–70 keV, the agreement with experiment is good. In Fig. 2 are plotted the differential cross

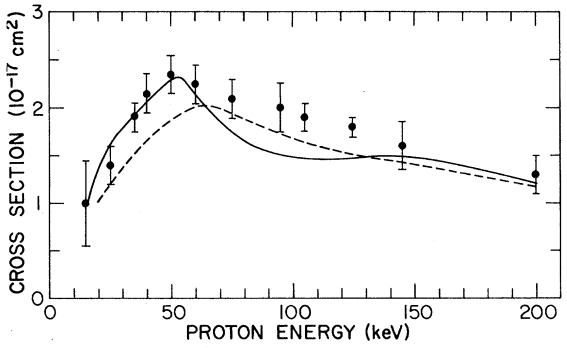

FIG. 3. Total cross sections for direct excitation to the $n=3$ level. ——, present results; — — —, results of calculations based on the Glauber approximation (Refs. 11 and 12); ●, experimental results of Park *et al.* (Ref. 8, renormalized as in Fig. 1).

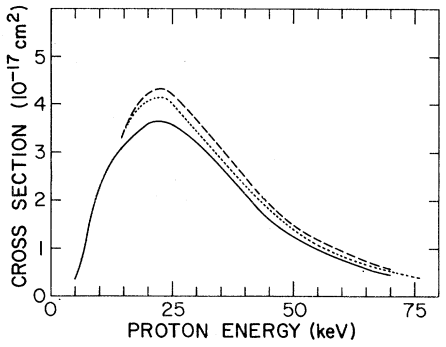

FIG. 4. Total cross sections for charge transfer to the $2s$ state. — — —, present results; — — —, earlier Sturmian results (Ref. 2); ——, experimental data of Bayfield (Ref. 13).

sections for excitation to the $n=2$ level at selected energies. These differential cross sections were obtained by using the phase information contained in the calculated transition amplitudes in an eikonal approximation. This procedure has been discussed in detail by Wilets and Wallace[9] and is equivalent to the passage from ray optics to wave optics by means of an imaginary Fraunhoffer screen; the relevant equations are (51) and (52) of Ref. 9. Also plotted in Fig. 2 are the experimental data of Park *et al.*[10] The angular distributions have very little structure. The agreement with experiment is reasonably good at 15 and 60 keV, but rather poor at 145 keV.

In Fig. 3 are plotted the present results for direct excitation to the $n=3$ level, together with the experimental data[8] and the results of calculations[11,12] based on the Glauber approximation. (The experimental data has the same normalization as in Fig. 1.) The agreement between the present results and the experimental data is reasonably good, but not significantly better than the agreement between the Glauber and experimental results, though the latter agreement may be fortuitous.

In Fig. 4 are plotted the present results for charge transfer to the $2s$ state, along with the 12-state Sturmian results[2] and the experimental results of Bayfield.[13] The error margin in the experimental results is about ±35% and the rather close agreement between the Sturmian results and the present results indicates that the latter are probably quite accurate.

The ionization cross section is obtained as follows: The probability, at a given impact parameter and energy, for a particular normalized eigenvector to be occupied at the end of the collision is multiplied by the square of the overlap matrix element of the eigenvector with the con-

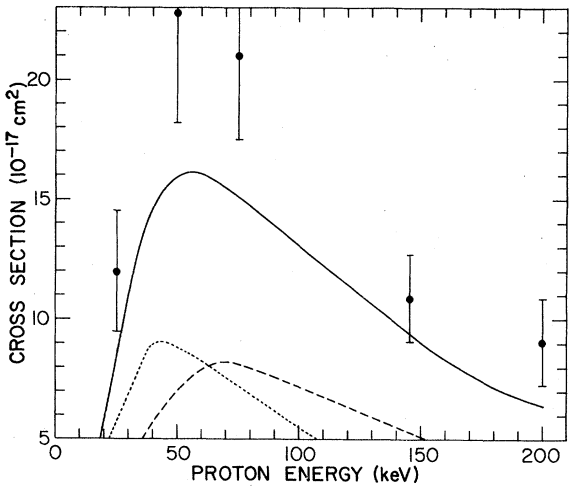

FIG. 5. Total cross sections for ionization. ——, present results; ●, experimental results of Park *et al.* (Ref. 14, renormalized as in Fig. 1); — — —, theoretical contribution from direct ionization; ····, theoretical contribution from charge transfer to the continuum. The solid curve is the sum of the contributions from direct ionization and charge transfer to the continuum. (Note that the vertical scale begins at 5×10^{-17} cm^2 and not at zero.)

tinuum of the hydrogen atom about whose nucleus the eigenvector is centered. The ionization probability is then obtained by summing such products over all eigenvectors. (This does not result in double-counting since the eigenvectors are linearly independent.) It is natural to divide the ionization probability into two separate contributions, namely, a *direct* ionization probability obtained by summing over just those eigenvectors centered about the target nucleus, and a probability for *charge transfer to the continuum* (abbreviated to CTTC) obtained by summing over those eigenvectors centered about the projectile nucleus. Integrating over all impact parameters then yields separate cross sections for direct ionization and for CTTC. This procedure has been discussed in detail in Ref. 2. The cross sections for direct ionization and for CTTC are plotted in Fig. 5, along with the present estimates of the total ionization cross section and the experimental data of Park *et al.*[14] Although the theoretical and experimental data are qualitatively in good agreement, the theoretical estimates lie well below the experimental data, expecially in the energy region near the peak in the total ionization cross section; this is probably due to the neglect of $l=3$ and higher partial waves in the calculation. Note that according to the present results the cross section for CTTC is larger than the cross section for direct ionization at energies below about 60 keV. This is remarkable and indicates that any ionization approximation which neglects CTTC will, for p-H scattering, be inadequate at energies below about 100 keV. The position of the peak in the CTTC cross section can be understood as follows: the probability for CTTC to occur maximizes when the velocity of the ejected electron is equal to the velocity of the projectile or, more precisely, when the internal energy of the electron-projectile subsystem is finally zero. Let m and M denote the electron and proton masses, respectively; corrections of the order m/M will be neglected. Working in the lab frame, let the $\hbar q$ and ϵ denote the initial momentum and energy of the electron, $\vec{v}$ the initial velocity of the projectile, and $\vec{u}$ the final velocity of the electron-projectile subsystem. Neglecting any momentum transferred to the target nucleus during the collison, it follows from momentum and energy conservation that if the electron-projectile subsystem finally has zero

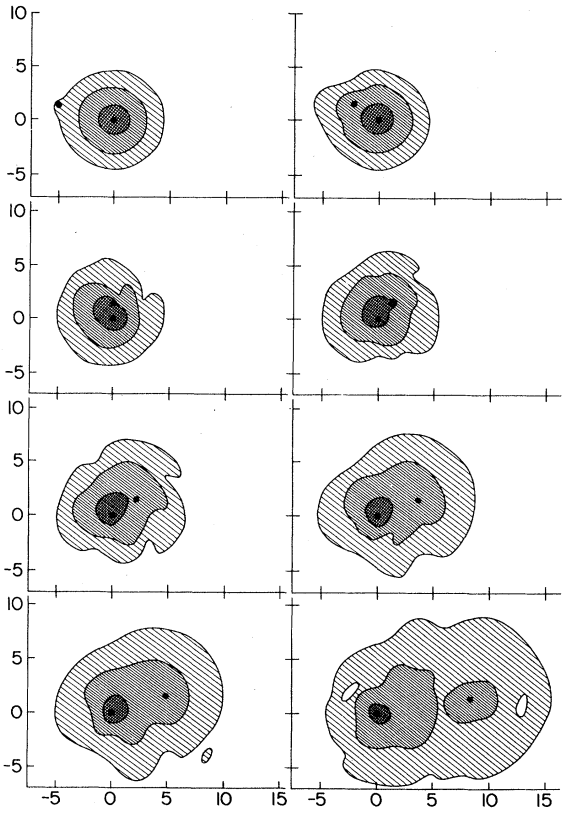

FIG. 6. Development of the charge distribution with time in the lab frame. The incident proton has a lab energy of 40 keV and an impact parameter of 1.5 a.u. The two protons are represented by black dots. The shading represents the relative electron density. The plane of the paper is the scattering plane of the collision, and the electron charge density has been integrated in the direction perpendicular to the scattering plane. Distances are measured in atomic units.

internal energy,

$$M\vec{v}+\hbar\vec{q}=(M+m)\vec{u}\,, \tag{2.1}$$

$$\tfrac{1}{2}Mv^2+\epsilon=\tfrac{1}{2}(M+m)u^2\,. \tag{2.2}$$

Eliminating $\vec{u}$ from Eqs. (2.1) and (2.2) and neglecting corrections of order m/M gives

$$v^2-(2\hbar/m)\vec{v}\cdot\vec{q}+2\epsilon/m=0\,. \tag{2.3}$$

Define μ by $\vec{v}\cdot\vec{q}=vq\mu$. Solving Eq. (2.3) for v and using atomic units ($\hbar=m=1$, $\epsilon=-\frac{1}{2}$) it follows that

$$v=\mu q+(\mu^2q^2+1)^{1/2} \tag{2.4}$$

and hence that

$$v^2=2\mu^2q^2+1+2\mu q\,(\mu^2q^2+1)^{1/2}\,. \tag{2.5}$$

The square of the momentum transform of the initial 1s wave function of the electron is, in atomic units, $(8/\pi^2)(1+q^2)^{-4}$. Hence the average value of v^2 is

$$\langle v^2\rangle=\int d^3q\,\frac{8}{\pi^2(1+q^2)^4}\left[2\mu^2q^2+1+2\mu q(\mu^2q^2+1)^{1/2}\right]$$

$$=\tfrac{5}{3}\text{ a.u.} \tag{2.6}$$

Therefore the energy at which the cross section for CTTC is expected to maximize is $\frac{1}{2}M\langle v^2\rangle\approx 42$ keV. This prediction is in excellent agreement with the result of Fig. 5.

In Fig. 6 is plotted the charge distribution of the electron as a function of time during the collision. The energy and impact parameter of the projectile are 40 keV and 1.5 a.u., respectively. The target proton remains at rest while the projectile moves with constant velocity. The plane of the paper is the scattering plane and the charge distribution has been integrated along the direction perpendicular to this plane. This figure illustrates the electron being dragged along by the projectile; the distortion of the electron cloud is considerable. Capture has clearly occurred in the last frame. The two holes in the electron cloud, in the last frame, may be artifacts of the approximations used.

While the results of the calculations presented here are, overall, presumably the most accurate currently available, the agreement with experiment is not entirely satisfactory. As mentioned above, part of the discrepancy may be due to the inability of the electron to escape to infinity within the framework of the square-integrable basis set used. This deficiency might be simply remedied by switching to a much larger basis set when the two protons move apart beyond a distance R_0, with R_0 chosen so that exchange matrix elements can be neglected and the larger number of basis functions handled with comparative ease. Elaborate calculations of proton–hydrogen-atom cross sections, based on a new method,[15] are currently being performed by Morrison and Öpik; it should be interesting to compare these results with the present ones.

ACKNOWLEDGMENTS

It is a pleasure to thank Dr. S. P. Rountree for his assistance with certain details of the computation. This work was supported by the Center for Energy and Mineral Resources at Texas A&M University and by the National Science Foundation under Grant No. PHY77-07406.

[1]D. F. Gallaher and L. Wilets, Phys. Rev. 169, 139 (1968).
[2]R. Shakeshaft, Phys. Rev. A 14, 1626 (1976).
[3]S. E. Lovell and M. B. McElroy, Proc. R. Soc. London Ser. A 283, 100 (1965).
[4]L. Wilets and D. F. Gallaher, Phys. Rev. 147, 13 (1966).
[5]I. M. Cheshire, D. F. Gallaher, and A. J. Taylor, J. Phys. B 3, 813 (1970).
[6]D. Rapp and D. Dinwiddie, J. Chem. Phys. 57, 4919 (1972).
[7]R. Shakeshaft, J. Phys. B 8, 1114 (1975).
[8]J. T. Park, J. E. Aldag, J. M. George, and J. L. Peacher, Phys. Rev. A 14, 608 (1976).
[9]L. Wilets and S. J. Wallace, Phys. Rev. 169 84 (1968).
[10]J. T. Park, J. E. Aldag, J. L. Peacher, and J. M. George, Phys. Rev. Lett. 40, 1646 (1978).
[11]V. Franco and B. K. Thomas, Phys. Rev. A 4, 945 (1971).
[12]K. Bhadra and A. S. Ghosh, Phys. Rev. Lett. 26, 737 (1971).
[13]J. E. Bayfield, Phys. Rev. 185, 105 (1969).
[14]J. T. Park, J. E. Aldag, J. M. George, J. L. Peacher, and J. H. McGuire, Phys. Rev. A 15, 508 (1977).
[15]H. G. Morrison and U. Öpik, J. Phys. B 14, 473 (1978).